

Quantum-limited laser frequency-modulation spectroscopy

Manfred Gehrtz* and Gary C. Bjorklund

IBM Research Laboratory, San Jose, California 95193

Edward A. Whittaker

Stevens Institute of Technology, Hoboken, New Jersey 07030

Received March 15, 1985; accepted May 30, 1985

Frequency-modulation (FM) spectroscopy permits high-resolution, high-sensitivity, easily calibrated absorption measurements of atomic and molecular species and narrow spectral features in solids. This paper reviews some important developments in laser FM spectroscopy, from its inception as a spectroscopic tool to the demonstration of quantum-limited absorption measurements, emphasizing the sensitivity limitations caused by residual amplitude modulation (RAM). Moreover, a detailed account is presented of a new double-beam, single-detector technique that efficiently suppresses the RAM and permits quantum-limited performance to be achieved in laser FM spectroscopy. We also include some recent results of the first reported FM spectroscopic investigations of the NO₂ molecule.

1. INTRODUCTION

Tremendous progress has been made recently in the development of high-resolution, high-sensitivity methods of optical spectroscopy. These advances were made possible by the high brightness and the narrow bandwidth of tunable-laser sources. In this paper we chronicle the progress of one such technique, laser frequency-modulation (FM) spectroscopy,^{1,2} which has permitted high-resolution absorption spectroscopy with quantum-limited detection sensitivity. This is not intended to be a comprehensive review of *all* developments in this field³ such as recent theoretical work⁴ or the use of pulsed lasers⁵ or multimode lasers⁶ in FM spectroscopy. We will limit ourselves to a discussion of those results that have attempted to exploit the high-sensitivity aspects of laser FM techniques. We present a unified treatment of laser FM spectroscopy, emphasizing the sensitivity limitations caused by residual amplitude modulation (RAM). We review previous efforts to overcome these limitations, which all relied on specific sample properties. We finally discuss in some detail a new, sample-independent technique that eliminates the baseline and noise problems resulting from the RAM and demonstrates quantum-limited sensitivity in laser FM spectroscopy.

We may understand the motivation for developing specialized techniques for direct absorption spectroscopy (i.e., the direct measurement of the optical attenuation of a light beam through an absorbing sample) through some general considerations of the signal-to-noise ratio (SNR) requirements. The signal in such a measurement is a detector photocurrent that is proportional to the optical intensity incident upon the photodetector and may be symbolically written as

$$S = \kappa I. \quad (1.1)$$

Here, κ represents the net attenuation of the laser intensity I incident upon the absorbing sample. It is implicitly a function of laser wavelength and may also be a function of time, depending on the particular detection scheme used. Noise contributions may usefully be separated into three

terms. From the detection electronics there will be a term independent of optical intensity (N_e). Detector shot noise will contribute a term proportional to the square root of the intensity ($\beta\sqrt{I}$). Finally, the nonideal light source will contribute an amplitude-fluctuation background term proportional to the optical intensity ($N_s I$). The SNR may then be written as

$$\text{SNR} = \frac{\kappa I}{[N_e^2 + (\beta\sqrt{I})^2 + (N_s I)^2]^{1/2}}. \quad (1.2)$$

As the intensity I increases, the SNR increases proportionally to I until the I -dependent terms in the denominator of Eq. (1.2) exceed N_e . The SNR will then saturate at some value of I that depends on the relative values of β and N_s . We say that a measurement is quantum limited if there is a range of I where the term $\beta\sqrt{I}$ dominates the SNR.

With both conventional and laser sources there is usually no such region for I because of large N_s . One way of surmounting this problem is to modulate the absorption κ and to detect phase sensitivity at the modulation frequency. As β is independent of frequency and the other terms are normally decreasing functions of frequency, it may be possible to move in detection frequency space to a quantum-limited regime. This is sometimes referred to as sample-modulation spectroscopy and has been applied quite successfully, particularly with conventional light sources.⁷⁻⁹ However, with tunable cw dye lasers, the source fluctuations extend to megahertz frequencies,¹⁰ and most samples are not easily modulated so rapidly. Indeed, high-frequency-modulated four-wave mixing¹¹ and the new technique of high-resolution ultrasonic modulation of persistent spectral holes^{12,13} are examples of the rare cases in which sample modulation in the megahertz range has been successfully employed in high-resolution spectroscopy. There are many situations of interest, however, in which the sample may not be modulated at all. In those cases we must resort to some type of source modulation.

Simple source-intensity amplitude modulation will not

suffice, as this imparts a time dependence to I , which is common to both the numerator and the denominator in Eq. (1.2). However, by using source *phase or frequency* modulation, one may effectively modulate the absorption-dependent signal κI without modulating the noise terms in Eq. (1.2). There are two closely related ways of accomplishing this. In wavelength-modulation spectroscopy (WMS), the source wavelength is varied with time. During alternate half-cycles of the modulation, the source samples the absorption at differentially separated wavelengths, and a derivative spectrum is obtained. This has been successfully applied to both conventional and laser sources.^{8,14} High-frequency WMS has been conducted with GaAlAs lasers,¹⁵ but, to our knowledge, quantum-limited performance has not been demonstrated with WMS so far.

For high resolution in the visible part of the spectrum, it has proved more convenient to impart a FM to the laser using an electro-optic modulator external to the laser source. The essential difference between wavelength modulation and FM may be understood in terms of the so-called modulation index M . Both methods add a time-dependent phase shift $\Delta\phi(t)$ to the light source, given by

$$\Delta\phi(t) = M \sin \Omega t. \quad (1.3)$$

As will be discussed in detail below (Subsection 2.A), this time-dependent phase shift results in an optical-frequency spectrum characterized by two or more sidebands. The sidebands are spaced from the optical carrier by multiples of the modulation frequency Ω . The distinction between wavelength modulation and FM is somewhat semantic, but we may usefully separate the two by the size of the modulation index and the size of the sideband spacing relative to the width of absorption features of interest (Γ_{feature}). In wavelength modulation the modulation index is very large, but the modulation frequency is low enough that the sideband spacing Ω is small compared with the spectroscopic feature under study:

$$\Omega \ll \Gamma_{\text{feature}}. \quad (1.4)$$

The spectroscopic feature is thus probed by many sidebands in WMS. In this case it is useful to consider the instantaneous frequency shift, which is the time derivative of $\Delta\phi(t)$ in Eq. (1.3):

$$\Delta\omega(t) = \Omega M \cos \Omega t = \Delta\omega_0 \cos \Omega t. \quad (1.5)$$

The maximum frequency excursion $\Delta\omega_0$ determines the resolution in laser WMS. One generally sets

$$\Delta\omega_0 < \Gamma_{\text{feature}}, \quad (1.6)$$

thus assuring a derivativelike spectrum.

In FM, the modulation index M is less than unity, but the modulation frequency is so high (in the radio-frequency regime, $\Omega = \omega_{\text{rf}}$) that the sideband spacing is of the order of the spectroscopic feature width

$$\Omega \sim \Gamma_{\text{feature}}. \quad (1.7)$$

The spectroscopic feature is thus probed by only one or two sidebands in FM spectroscopy. In the remainder of this paper we will highlight some of the difficulties encountered in putting high-sensitivity laser FM spectroscopy into practice and review some of the important measurements made so far.

Before continuing, we should point out that there have arisen a wide variety¹⁶ of laser techniques that allow high sensitivity and high resolution. With the exception of direct absorption, these methods monitor some indirect effect of the optical absorption and include laser-induced fluorescence,¹⁷ optoacoustic spectroscopy,¹⁸ and optogalvanic spectroscopy.¹⁹ Laser intracavity absorption is also capable of high sensitivity.²⁰ A quantitative comparison of each of these methods is made difficult by the varying regimes of applicability of each technique. Let us emphasize here the main virtues of extracavity direct-absorption spectroscopy and recognize that the applicability of all methods depends on the goals and conditions of the desired measurement. Extracavity absorption spectroscopy allows a simple calibration procedure, high resolution, remote-sensing possibilities, and sensitivity to any absorption regardless of the ultimate disposition of the absorbed energy. The main disadvantages include line-of-sight averaging of the sample absorptivity, a quantum-limited sensitivity, which, in general,^{21,22} will be inferior to that of methods that may monitor photon emission, and, finally, sensitivity to differential absorption rather than absolute absorption when modulation methods are applied.

2. LASER FREQUENCY-MODULATION SPECTROSCOPY

Laser FM techniques have been developed as a means for fast readout¹ of optical hole-burning memories²³ and independently as a servolocking technique for tunable lasers.² FM techniques have been employed successfully in a wide variety of applications³ that require high-resolution, high-sensitivity spectroscopy. In this section, the basic notations of FM spectroscopy are reviewed, emphasizing the detection-sensitivity limit that can be achieved with this technique. Moreover, we present a compilation of the formalism of FM spectroscopy in such detail that the sensitivity problems associated with imperfect phase modulation can be rigorously analyzed in later sections. The following description will be limited to implementations of the FM technique that use phase modulators external to the laser source; here we do not refer explicitly to the recently demonstrated high-frequency heterodyne spectroscopy with diode lasers that employs internal FM by direct injection-current modulation.^{24,25}

A. Basics of Laser Frequency-Modulated Spectroscopy

The principle of FM spectroscopy and the basic setup are illustrated in Fig. 1. A single-frequency laser generates radiation at the optical-carrier frequency ω_c . Using complex notation (where the physical field amplitudes are given by the real part of the complex quantities shown below), the electric field is

$$E_1(t) = E_0 \exp(i\omega_c t). \quad (2.1)$$

The beam is passed through an electro-optic phase modulator (EOM) driven at frequency ω_{rf} by a sinusoidally varying radio-frequency (rf) field.²⁶ The spectrum after the modulator is described by

$$\begin{aligned} E_2^F(t) &= E_0 \exp[i(\omega_c t + M \sin \omega_{\text{rf}} t)] \\ &= E_0 \sum_{n=-\infty}^{n=\infty} J_n(M) \exp[i(\omega_c + n\omega_{\text{rf}})t], \end{aligned} \quad (2.2)$$

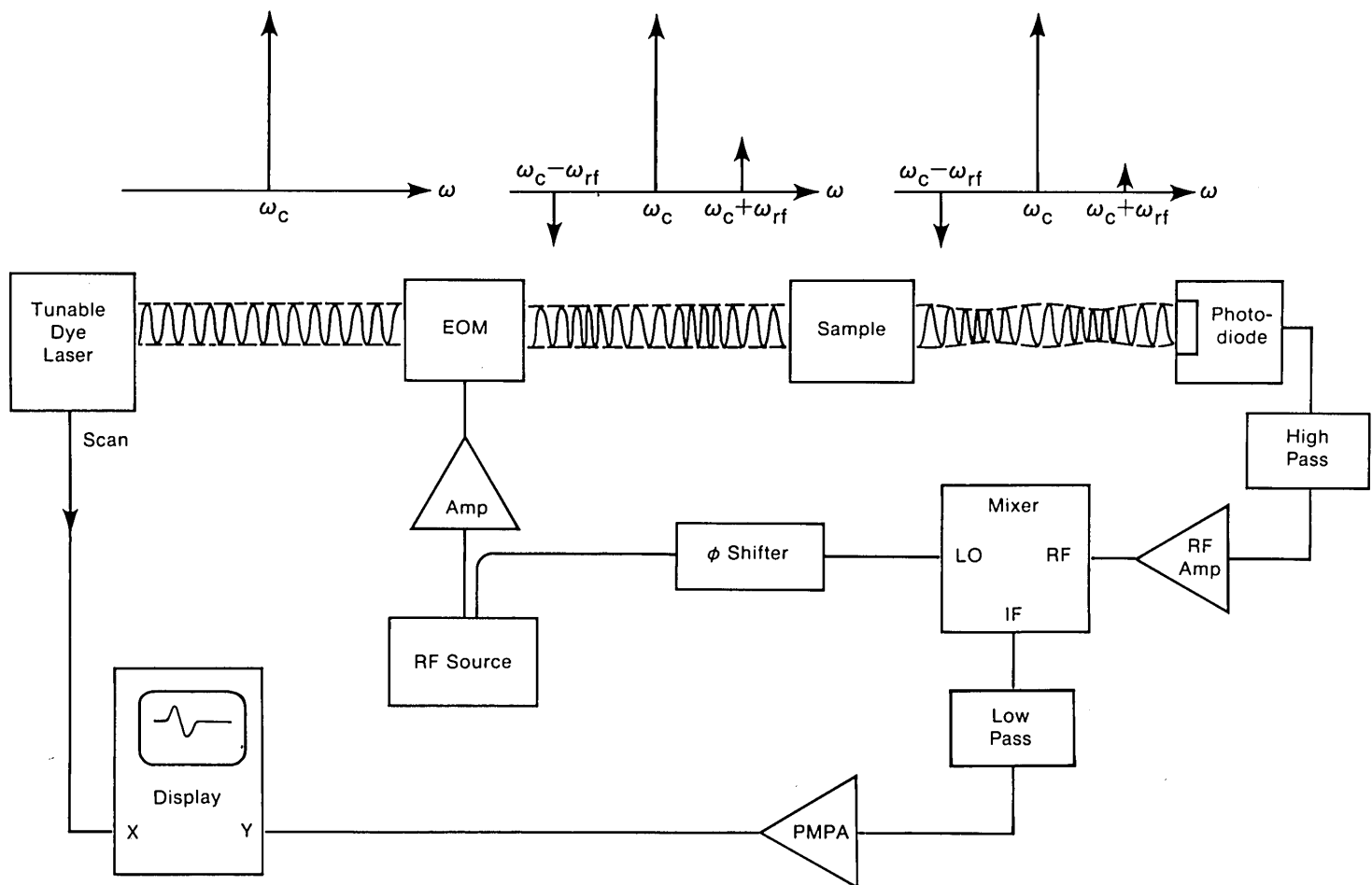


Fig. 1. Schematic diagram illustrating the principle of FM spectroscopy and the basic setup used in the experiments.

where M is the modulation index and the J_n are Bessel functions of order n . Note that we specifically use ω_{rf} for the (general) modulation frequency Ω defined earlier (Section 1). In the ideal case of pure FM the intensity of the beam is constant:

$$I_2^F(t) = \frac{cE_0^2}{8\pi} = I_0. \quad (2.3)$$

For the further discussion it will be assumed that the modulation index is small compared with unity, so that the FM spectrum can be described by a strong carrier at frequency ω_c and two weak sidebands at frequencies $\omega_c \pm \omega_{\text{rf}}$:

$$E_2^F(t) = E_0 \left\{ \frac{M}{2} \exp[i(\omega_c + \omega_{\text{rf}})t] + \exp(i\omega_c t) - \frac{M}{2} \exp[i(\omega_c - \omega_{\text{rf}})t] \right\}. \quad (2.4)$$

Higher-order sidebands are negligible in the small modulation-index limit. We note here that the superscript F used in this section is necessary to distinguish the pure-FM case presented here from the extension to the more complicated case of imperfect phase modulation in later sections.

The beam is next passed through a sample of length L , characterized by an intensity-absorption coefficient α and an index of refraction η , which are both functions of the optical frequency. It is convenient to use the complex quantities

$$T_n = \bar{T} \exp(-\delta_n - i\phi_n), \quad (2.5)$$

where

$$\delta_n = \alpha_n L/2, \quad \phi_n = \eta_n L(\omega_c + n\omega_{\text{rf}})/c. \quad (2.6)$$

The subscript $n = 0, \pm 1$ specifies the values at $\omega_c, \omega_c \pm \omega_{\text{rf}}$. Thus δ_n denotes the amplitude attenuation, and ϕ_n denotes the optical phase shift experienced by each frequency component in the FM spectrum [Eq. (2.4)]. The pre-exponential factor in Eq. (2.5) accounts for a possible broadband background:

$$\bar{T} = \exp(-\bar{\delta} - i\bar{\phi}), \quad (2.7)$$

where neither the background amplitude attenuation $\bar{\delta}$ nor the background optical phase shift $\bar{\phi}$ changes on the scale of the FM spectrum in Eq. (2.4).

The transmitted field is

$$E_3^F(t) = E_0 \left\{ T_0 \exp(i\omega_c t) + T_1 \frac{M}{2} \exp[i(\omega_c + \omega_{\text{rf}})t] - T_{-1} \frac{M}{2} \exp[i(\omega_c - \omega_{\text{rf}})t] \right\}. \quad (2.8)$$

In high-sensitivity FM spectroscopy one generally deals with weak, narrow-band spectral features that are characterized by all $\delta_0, \delta_0 - \delta_1, \delta_0 - \delta_{-1}, \phi_0 - \phi_1, \phi_0 - \phi_{-1}$ being small compared with unity. In this case the transmitted intensity simplifies to¹

$$I_3^F(t) = F(t) = I_0 \exp(-2\bar{\delta})(1 - \Delta\delta M \cos \omega_{\text{rf}}t + \Delta^2 \phi M \sin \omega_{\text{rf}}t), \quad (2.9)$$

where we introduce the abbreviation $F(t)$ for later use and where

$$\Delta\delta = \delta_1 - \delta_{-1}, \quad \Delta^2\phi = (\phi_1 - \phi_0) - (\phi_0 - \phi_{-1}). \quad (2.10)$$

Terms induced by interaction of higher-order FM sidebands with the spectral feature²⁷ have been neglected in our small modulation-index approximation.

The quadrature component ($\cos \omega_{rf}t$) is proportional to the difference in loss experienced by the upper and the lower sidebands, and the in-phase component ($\sin \omega_{rf}t$) is proportional to the difference between the phase shift experienced by the carrier and the average of the phase shifts experienced by the sidebands. The physical meaning of the differences defined in Eqs. (2.10) can be most easily deduced in the wavelength-modulation limit (cf. Section 1). Here, the quadrature component becomes proportional to the derivative of the absorption, whereas the in-phase component becomes very small and is proportional to the second derivative of the dispersion.

The evolution of the electric-field amplitude spectrum along the beam path is schematically illustrated in the top of Fig. 1. One recognizes that the essential consequence of the differential absorption (or phase shift) caused by the sample is an unbalancing of the sideband amplitudes: Compare the pure-FM spectrum in Eq. (2.4) with the spectrum after the sample [Eq. (2.8)] and recall that $T_1 \neq T_{-1}$.

B. Recording of Laser Frequency-Modulation Spectra

When a narrow-band absorption feature causes the differences $\Delta\delta$, $\Delta^2\phi$ in Eqs. (2.10) to be nonzero, the beam emerging from the sample is amplitude modulated, i.e., its intensity is no longer constant [cf. Eq. (2.3)] as a consequence of the FM-AM conversion by the spectral feature. The beam finally impinges on a high-speed photodetector, generating an electric signal that contains beat notes at the modulation frequency ω_{rf} . These beat signals are subsequently detected using standard rf signal-processing techniques (cf. Fig. 1): The photosignal is directed to a double-balanced mixer that is fed by a local oscillator (LO) derived from the same rf source that is used to drive the EOM. A phase shifter (ϕ shifter) permits the phase of the LO to be set such that either the quadrature or the in-phase portion of the photosignal is detected. When the laser wavelength is scanned with the modulation frequency ω_{rf} held constant, either an absorptive or a dispersive FM spectrum is obtained at the mixer intermediate-frequency (IF) output. Here and in what follows we use the wavelength $\lambda = \lambda_c = 2\pi c/\omega_c$ rather than the optical carrier frequency ω_c for brevity. A detailed line-shape analysis can be found in Refs. 27 and 28. The mixer output is proportional to

$$\hat{F}(\lambda) = I_0 \exp(-2\bar{\delta}) \times \begin{cases} -\Delta\delta M & \text{(quadrature),} \\ \Delta^2\phi M & \text{(in phase)} \end{cases} \quad (2.11)$$

where the caret (^) on $\hat{F}(\lambda)$ denotes either the quadrature or the in-phase Fourier component of $F(t)$ in Eq. (2.9). When no absorbing sample is present, the corresponding mixer output signal is zero. This zero background signal can be viewed as being due to a perfect cancellation of the two rf signals arising from the upper and the lower sidebands beating against the carrier. On the other hand, when a narrow-band spectral feature upsets this balance, a net rf beat signal at the photodetector output is obtained, which is subsequently demodulated to yield $\hat{F}(\lambda)$.

C. Detector-Sensitivity Limit of Laser Frequency-Modulation Spectroscopy

The principal advantages of using FM techniques in high-resolution, high-sensitivity spectroscopy are twofold. One is the zero background obtained when no narrow-band spectral feature is present that would upset the FM sideband balance. The second advantage originates in the high modulation frequencies employed in FM spectroscopy. Generally, ω_{rf} is in the range of several hundred to several thousand megahertz. This translates the detected signal frequency [Eq. (2.9)] well beyond the maximum frequency of laser power fluctuations¹⁰ into the shot-noise-dominated regime. As a consequence, shot-noise- (quantum-) limited performance should be readily achievable even with notoriously noisy dye lasers when FM techniques are employed.

In a detailed SNR analysis, Bjorklund *et al.*²⁸ accounted for this quantum-limited feature of FM spectroscopy. The central result of the analysis is the minimum differential absorption $\Delta\delta_{min}$ that can be detected under shot-noise-limited conditions:

$$\Delta\delta_{min} = \frac{2}{M} \left[\frac{\Delta f}{\epsilon(I_0/h\omega_c)} \right]^{1/2}. \quad (2.12)$$

Here ϵ is the photodetector quantum efficiency, and Δf is the bandwidth of the detection electronics. Assuming that $\epsilon = 1$, $I_0 = 5$ mW, $M = 0.1$, and $\Delta f = 1$ Hz, the detection-sensitivity limit of an FM-spectroscopy experiment is predicted to be $\Delta\delta_{min} = 1.5 \times 10^{-7}$. It should be pointed out, however, that the sensitivity can be readily improved (at least in principle) by using higher light powers and stronger modulation indices.

According to the theoretical prediction of Eq. (2.12), the minimum detectable differential absorptivity $\Delta\delta_{min}$ is proportional to the square root of the detection bandwidth Δf . This dependence, which is typical of a noise-limited sensitivity, is schematically shown in Fig. 2 (dashed line).

The main problems encountered in attempting actually to achieve quantum-limited performance in FM spectroscopy according to Eq. (2.12) will be discussed in the following sections. Here, an additional experimental detail should be emphasized that has to be observed in these attempts: The

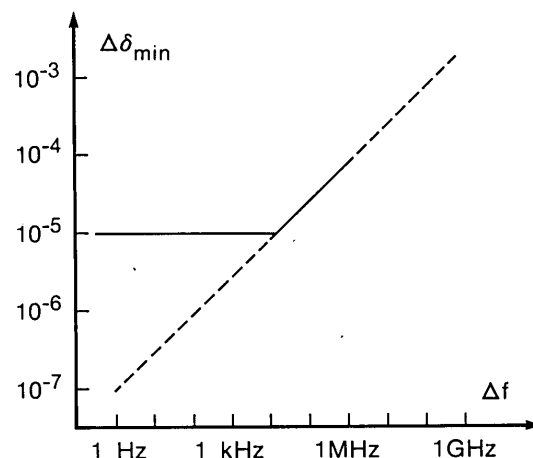


Fig. 2. Minimum detectable (SNR = 1) differential absorptivity $\Delta\delta_{min}$ as a function of detection bandwidth Δf . The diagram schematically illustrates the sensitivity limit of FM spectroscopy under background-limited conditions (solid line; cf. Subsection 2.D). The theoretical prediction according to Eq. (2.12) is shown as the dashed line.

electronic low-frequency noise spectrum caused by the laser power fluctuations has fairly strong components that can easily leak at appreciable levels through commercial rf amplifiers and mixers. We have observed noise levels at the mixer IF output caused by this leakage that were up to 20 dB above the shot-noise level. Apart from being inconsistent with shot-noise calculations, this excess noise is readily distinguished from the quantum noise by its different light power dependence ($\propto I_0$). It is therefore essential that an additional high-pass (or bandpass) filter be inserted into the rf detection path (cf. Fig. 1).

D. Experimental Tests of the Detection Limit of Frequency-Modulation Spectroscopy

The first serious attempt to quantify the practically achievable detection limit was made by Whittaker *et al.*²⁹ In that series of experiments, FM spectroscopy was used to measure sodium D-line absorption in an atomic-absorption-spectroscopy-type burner aspirated with dilute NaCl solutions. The results illustrated the width dynamic range, the linearity, and the ease of calibration achievable with FM spectroscopy. Perhaps the most important result of this work was the observation that the lower sensitivity limit was set not by the detector shot noise but by RAM imparted to the laser beam by the imperfect EOM. This was evidenced by the appearance of fringes in the laser frequency scans at the highest sensitivity measurements. These fringes were interpreted as some type of étalon effect in the EOM itself. A lower differential-absorption sensitivity limit of 1.5×10^{-4} was quoted in Ref. 29. This practical limit is caused by a detection-bandwidth-independent (coherent) *background* signal, in contrast to the theoretical detection limit in Eq. (2.12), which describes a *noise-limited* sensitivity.

As will be shown in detail in Section 3, the RAM induces a background signal that is given by the modulation index and the incident light power. At very narrow detection bandwidths, the noise level (which is proportional to $\sqrt{\Delta f}$) is lower than the coherent RAM background level. In this narrow-detection-bandwidth regime, the sensitivity is *background limited* and does not depend on Δf . With increasing detection bandwidth, the noise level finally becomes higher than the background level, and, in this wide-detection-bandwidth regime, the sensitivity is *noise limited* and does depend on Δf according to Eq. (2.12). This behavior is schematically illustrated in Fig. 2 (solid line).

In fact, near-quantum-limited sensitivity has been demonstrated in the medium-detection-bandwidth regime: Hollberg *et al.*³⁰ used Doppler-free nonlinear saturated absorptions and dispersions of iodine vapor as a study case for investigating the sensitivity limit of FM spectroscopy. With potential applications of FM techniques for laser frequency locking² in mind, these workers employed a detection bandwidth $\Delta f = 20$ kHz. For a 5% deep saturation hole in a 10% iodine absorption line, they achieved a SNR = 75, which was within a factor of 2 of the theoretical shot-noise limit (predicted from their experimental conditions).

It is important to realize, however, that this superb result *cannot be extrapolated* to narrow-bandwidth conditions (cf. Fig. 2). In applications in which ultrahigh sensitivity is required, i.e., in the narrow-bandwidth regime, the practical sensitivity is limited by coherent RAM-induced background signals. *Thus FM spectroscopy is not quantum limited in*

this regime. Before we propose and demonstrate a novel technique that overcomes this RAM-induced sensitivity limit and renders FM spectroscopy a quantum-limited tool especially in the important ultrahigh-sensitivity (i.e., narrow-bandwidth) regime, we will analyze next the origin and the consequences of the spurious RAM signals.

3. RESIDUAL AMPLITUDE MODULATION

In practice, pure phase (or frequency) modulation is difficult to achieve, and the FM laser beam is amplitude modulated even when no sample is present. Recently, the implications of this RAM have been discussed within the context of high-frequency heterodyne spectroscopy with diode lasers.^{24,25} In this application the diode laser is internally modulated by direct injection-current modulations; thus a relatively strong RAM signal always accompanies the FM. Here we analyze RAM-contaminated FM spectroscopy from a different point of view, emphasizing the peculiarities of external phase modulation with an EOM. The detailed formalism presented here will provide the framework for the development of a new technique discussed in Section 5 that overcomes the sensitivity problems associated with the RAM.

A. Effects of Residual Amplitude Modulation on Frequency-Modulation Spectra

Experimentally, the RAM manifests itself as an intensity modulation of the beam emerging from the EOM (even when no sample is present). Thus, in contrast to Eq. (2.3), the intensity of the beam after the modulator is time dependent:

$$I_2(t) = I_0[1 + 2R \sin(\omega_{\text{rf}}t + \psi)], \quad (3.1)$$

where both R and ψ are functions of the laser wavelength λ and the modulation frequency ω_{rf} , in general. The additional modulation term depends on the two parameters necessary to characterize the RAM: R denotes the strength of the RAM; it can be viewed as the RAM index (in analogy to the FM index M , introduced earlier). ψ is the phase shift of the RAM with respect to the FM [cf. Eq. (2.2)]. For the analysis that follows, the effects of the RAM on FM spectra are most usefully described in terms of the electric-field amplitude emerging from the EOM. This amplitude is no longer given by $E_2^F(t)$ (Eq. (2.2)], which is valid in the ideal case of pure FM (superscript F) but can be viewed as modified by an additional modulation term:

$$E_2(t) = E_2^F(t)[1 + R \sin(\omega_{\text{rf}}t + \psi)]. \quad (3.2)$$

To lowest order in R or ω_{rf} , this is in fact consistent with the observed intensity modulation [Eq. (3.1)].

In the limit of both the RAM and the FM index being small compared with unity and retaining only terms depending on the fundamental of the modulation frequency ω_{rf} , the FM-RAM spectrum is a sum:

$$E_2(t) = E_2^F(t) + E_2^A(t), \quad (3.3)$$

where the FM component (superscript F) is given by Eq. (2.2) and the AM component resulting from the RAM (superscript A) adds to the sidebands at $\omega_c \pm \omega_{\text{rf}}$:

$$E_2^A(t) = E_0 \left\{ \frac{R}{2i} \exp[i(\omega_c + \omega_{rf})t + i\psi] - \frac{R}{2i} \exp[i(\omega_c - \omega_{rf})t - i\psi] \right\}. \quad (3.4)$$

When the beam is now passed through the sample, both contributions interact with the spectral feature of interest [Eq. (2.5)]. The electric field after the sample is thus also a sum:

$$E_3(t) = E_3^F(t) + E_3^A(t), \quad (3.5)$$

where the FM component (superscript F) is given by Eq. (2.8), and the additional AM component (superscript A) arises from the interaction of the RAM-induced sidebands at $\omega_c \pm \omega_{rf}$ with the spectral feature:

$$E_3^A(t) = E_0 \left\{ T_1 \frac{R}{2i} \exp[i(\omega_c + \omega_{rf})t + i\psi] - T_{-1} \frac{R}{2i} \exp[i(\omega_c - \omega_{rf})t - i\psi] \right\}. \quad (3.6)$$

As a consequence, the intensity after the sample is a sum of several terms. To first order in M and R and retaining only components that depend on the fundamental of the modulation frequency ω_{rf} , one obtains

$$I_3(t) = F(t) + D(t) + \exp(-2\bar{\delta})B(t). \quad (3.7)$$

Here $F(t)$ denotes the ideal (pure) FM signal that is recorded when no RAM is present [Eq. (2.9)], and the distortive term arises because of the interaction of the RAM-induced sidebands with the spectral feature of interest

$$D(t) = -I_0 \exp(-2\bar{\delta}) [R(\Sigma\delta \sin \psi + \Delta\phi \cos \psi) \cos \omega_{rf}t + R(\Sigma\delta \cos \psi - \Delta\phi \sin \psi) \sin \omega_{rf}t], \quad (3.8)$$

where the difference $\Delta\phi = \phi_1 - \phi_{-1}$ is defined analogously to Eqs. (2.10) and the sum $\Sigma\delta$ is given by

$$\Sigma\delta = 2\delta_0 + \delta_1 + \delta_{-1}. \quad (3.9)$$

When plotted as a function of laser frequency, both the dispersive ($\Delta\phi$) and the absorptive ($\Sigma\delta$) signals have even symmetry around the molecular transition frequency. This is a contrast to FM spectra, where dispersive ($\Delta^2\phi$) and absorptive ($\Delta\delta$) signals have odd symmetry.²⁸

The background signal arises even when no sample is present:

$$B(t) = I_0(2R \sin \psi \cos \omega_{rf}t + 2R \cos \psi \sin \omega_{rf}t) = I_2 2R \sin(\omega_{rf}t + \psi). \quad (3.10)$$

Note that this term has to be multiplied by $\exp(-2\bar{\delta})$ when the beam is attenuated by a broadband background absorption [Eq. (3.7)].

The importance of the distortive term $D(t)$ as compared with the pure-FM term $F(t)$ may be estimated by assuming that the terms depending on the spectral feature under study (i.e., the differential absorptions and phase shifts) are approximately the same in $D(t)$ [Eq. (3.8)] and in $F(t)$ [Eq. (2.9)]. Then the distortive $D(t)$ term is weaker than the pure-FM term $F(t)$ by roughly the ratio R/M , which in many cases³¹ is less than 0.01 (see Section 4). We thus neglect the distortive term in the following analysis and approximate the intensity of the beam emerging from the sample

$$I(t) = F(t) + \exp(-2\bar{\delta})B(t). \quad (3.11)$$

When no sample is present (subscript ns) we get

$$I_{ns}(t) = I_0 + B(t). \quad (3.12)$$

As the carrier wavelength λ is scanned, the corresponding mixer output signals are proportional to

$$M(\lambda) = \hat{F}(\lambda + \exp(-2\bar{\delta})\hat{B}(\lambda)) \quad (3.13)$$

and

$$M_{ns}(\lambda) = \hat{B}(\lambda) \neq 0. \quad (3.14)$$

Here, $\hat{F}(\lambda)$ denotes the pure-FM signal that would be recorded if no RAM were present [Eq. (2.11)]. The caret ($\hat{\cdot}$) on the background signal $\hat{B}(\lambda)$ denotes the Fourier component of the corresponding time-dependent signal $B(t)$ [Eq. (3.10)] selected with the appropriate LO phase [analogous to the definition in Eq. (2.11)]:

$$\hat{B}(\lambda) = I_0 \times \begin{cases} 2R \sin \psi & \text{(quadrature)} \\ 2R \cos \psi & \text{(in phase)} \end{cases}. \quad (3.15)$$

The wavelength dependence of the background signal $B(\lambda)$ can originate in the RAM index $R(\lambda)$ as well as in the RAM phase shift $\psi(\lambda)$. In the following subsection we briefly review what is now known about the RAM parameters R and ψ in electro-optic phase modulation.

B. Residual Amplitude Modulation in Electro-Optic Phase Modulation

A careful analysis of the RAM problem in electro-optic phase (or frequency) modulation is presented in Ref. 32. There it was recognized that RAM may be resolved into two components, which are different in magnitude as well as in their dependence on laser wavelength. The strong component is due to an interference effect and exhibits a periodic dependence on laser frequency (fringes). The weak component is observed when interference effects are excluded (see below) and exhibits a much less pronounced dependence on laser wavelength. In many cases, this component turns out to be virtually independent of laser frequency. Evidence for this behavior is presented in Fig. 3.

The central result of the paper³² is that the fringes may be explained as a multipassing effect in the EOM: The EOM acts like a Fabry-Perot étalon filled with a dielectric whose index of refraction is being modulated. With this model, the dependence of the fringes on modulation phase and frequencies could be satisfactorily explained. Specifically, the RAM phase shift ψ defined in Eq. (3.1) was found to be independent of the laser wavelength λ . It is very small:

$$\Psi(\text{EOM}) \sim 0 \quad (3.16)$$

for modulation frequencies small compared with the free spectral range of the EOM crystal (viewed here as a Fabry-Perot interferometer):

$$\omega_{rf} \ll 2\pi\nu_{FSR}. \quad (3.17)$$

The RAM index $R(\lambda)$ was found proportional to the FM index M in Ref. 32. R strongly depends on the laser wavelength λ , giving rise to the observed fringes. The maximum RAM-index values (corresponding to the fringe peaks) are 2 to 3 orders of magnitude smaller than the FM index:

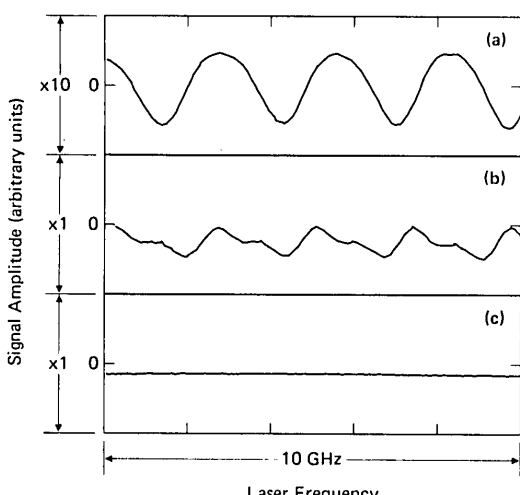


Fig. 3. RAM fringes obtained by scanning the laser frequency 10 GHz with no sample present. The EOM material used here was a LiTaO₃ crystal. (a) Laser beam orthogonal to crystal end face and $\omega_{rf} = 333$ MHz. (b) Laser beam orthogonal to crystal end face and $\omega_{rf} = 309$ MHz (equivalent to a $\pi/2$ phase shift at the rf mixer LO port), illustrating the well-defined phase of the fringe signal. (c) Laser beam angled by $\sim 3^\circ$ from normal to crystal end face and $\omega_{rf} = 309$ MHz. By appropriate choice of phase and beam orientation, the fringes may be completely eliminated, leaving a contribution to the RAM that for this crystal is virtually independent of laser frequency.

$$\frac{R(\text{multipass EOM})}{M} \sim 10^{-3} \dots 10^{-2}. \quad (3.18)$$

Any pair of parallel optical surfaces (other than the EOM end faces) will induce a fringe effect on the frequency-modulated laser beam. It was recognized in Ref. 32, however, that the modulation phase and frequency behavior differs from that of the EOM fringes. In the limit of small modulation frequency [cf. relation (3.17)] AM signals caused by such external surfaces are virtually in quadrature with the RAM signals caused by the EOM itself:

$$\psi(\text{external}) \sim \frac{\pi}{2}, \quad (3.19)$$

and this phase shift depends weakly on the laser wavelength λ . In both cases the fringes may be effectively reduced in amplitude by using Brewster-angled surfaces and antireflection coatings.

A much smaller RAM component is observed separately when multipassing effects are excluded (e.g., by angling the crystal end faces to the laser beam). This single-pass contribution is more difficult to analyze, particularly because its modulation phase behavior is not very reproducible. At least some part of it may come from the modulation of the Fresnel-reflection coefficients at the crystal-air interface, and this may also be reduced by antireflection coatings. Our understanding is, however, far from being satisfactory at present. Here we summarize a few experimental facts that emerged from recent observations in our laboratory. The amplitude of this contribution changes drastically when different EOM crystal materials are used (e.g., AD*P instead of LiTaO₃) as well as when different batches of the same EOM crystal material (LiTaO₃) are employed. The single-pass effect is quite small:

$$\frac{R(\text{single-pass EOM})}{M} \sim 10^{-5} \dots 10^{-3}. \quad (3.20)$$

It was also observed in these comparative experiments that for most LiTaO₃ crystals the beam emerging from the EOM has an inhomogeneous cross section when the RAM signal is monitored: Apparently the RAM phase is *not* constant across the beam. As a consequence, no LO phase setting could be found, in general, where the RAM signal could be completely nulled, and in many cases the signal turned out to depend on the laser frequency when inspected under higher sensitivity. This behavior was also quite irreproducible; specifically the observed laser frequency dependence varied drastically when the beam path through the EOM crystal was changed slightly. In summary, therefore, the small single-pass RAM contribution, which is observed when multipassing fringe effects are excluded (e.g., by angling the EOM crystal with respect to the input laser beam), is far from being understood satisfactorily.

C. Detection-Sensitivity Limitations Caused by Residual Amplitude Modulation

Independent of its actual origin, the RAM detrimentally affects both features of laser FM spectroscopy that were recognized as advantageous in high-resolution, high-sensitivity spectroscopic applications (cf. Subsection 2.C).

The first consequence of RAM is easily seen from Eqs. (3.13) and (3.14): The baseline encountered in RAM-contaminated FM spectroscopy is *not* zero. Depending on the wavelength dependence of the RAM index and phase shift, this baseline will also show a more or less pronounced laser wavelength dependence. The sensitivity limitations caused by a varying baseline are difficult to assess in general; e.g., a very sharp spectral feature might still be detectable in spite of a fairly strong baseline slope. One may arrive at some rough figure of merit for the baseline-induced sensitivity limit by using Eqs. (2.9) and (3.10) and estimating the differential absorption that would lead to an FM signal F of the same order of magnitude as the RAM-induced background signal B . It is readily concluded, then, that the ratios (R/M) quoted in relations (3.18) and (3.20) directly denote the sensitivity limitation caused by a RAM-induced nonzero baseline $B(\lambda)$:

$$\Delta\delta_{\min} \sim \frac{R}{M} \sim 10^{-5} \dots 10^{-2}. \quad (3.21)$$

We emphasize again that this is a background-induced limit that (below a certain detection bandwidth $\Delta f = 1 \dots 10$ kHz) does not depend on Δf . Apparently, this background limitation does not apply in cases in which the background is only weakly (or not at all) dependent on laser wavelength.

The second consequence of RAM, however, is operational whether the RAM-induced background is dependent on laser wavelength or not. This may be understood by referring to Fig. 4, which is an idealized power versus frequency spectrum of the modulated laser intensity. At low frequencies, the laser intensity exhibits large amplitude fluctuations. Beyond a certain maximum frequency (a few megahertz for many dye lasers), the fluctuation power spectrum becomes flat and approaches the shot-noise level.^{10,11} If no RAM-induced background signal were present, the noise spectrum around the modulation frequency ω_{rf} would be flat and quantum limited also, indicating that shot-noise-limited detection sensitivity is achievable with a pure-FM laser beam. With a RAM-contaminated FM beam, however, additional noise

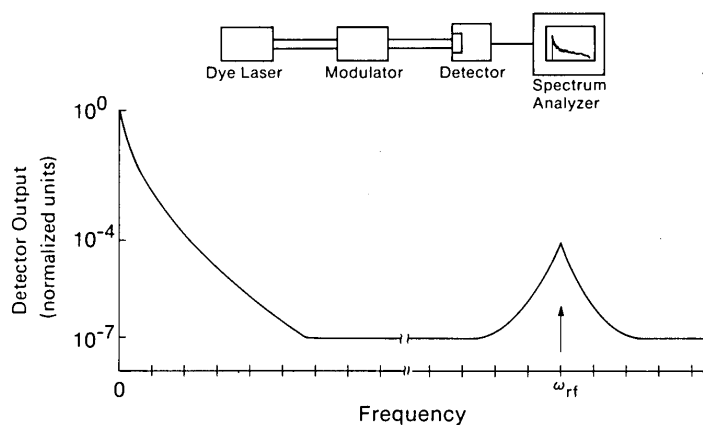


Fig. 4. Sketch illustrating the RAM background problem of FM spectroscopy. The figure shows the idealized power versus frequency spectrum of the photodetector signal (normalized to the zero-frequency value) in FM spectroscopy in the absence of any sample absorption. The peak at the modulation frequency ω_{rf} comes from the AM imparted by the imperfect phase modulator.

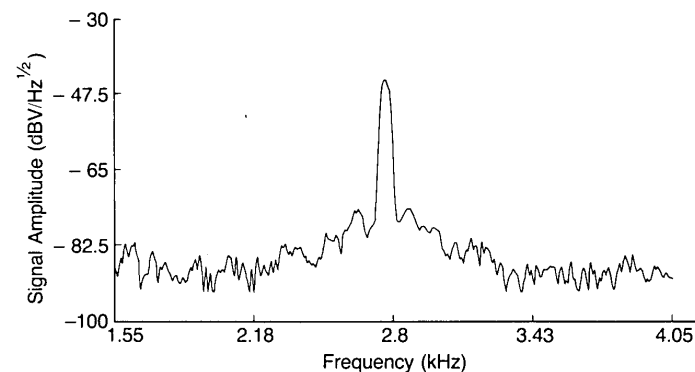


Fig. 5. Electronic power spectrum of the FM signal taken at the output of the rf mixer IF port. The modulation frequency was 2 GHz. The laser was mechanically chopped at 2.8 kHz. No sample was in the beam. The spectrum shows the RAM signal peaking at the chopper frequency, accomplished by the low-frequency noise spectrum leaking through via the RAM.

(in excess of the quantum noise) is observed around the modulation frequency ω_{rf} . The RAM effectively leaks an upconverted copy of the low-frequency noise spectrum through the modulator.

This spectrum is finally downconverted again by the rf mixer, yielding a low-frequency noise spectrum at the mixer output, which is an attenuated copy of the original power spectrum of the laser-intensity fluctuations. An experimental example of the low-frequency noise spectrum at the mixer output is shown in Fig. 5, which will be discussed in Section 4. As a consequence, one is faced with the same type of background-noise problem that one previously set out to eliminate with FM, although at a much lower level. The sensitivity limitation by this low-frequency noise feedthrough is difficult to assess in general because of its strong dependence on the power spectrum of the laser-intensity fluctuations. We have observed RAM-induced excess noise levels of up to 20 dB above the shot-noise floor. Clearly the additional noise leaking through via the RAM deteriorates the achievable SNR; as a consequence, shot-noise-limited sensitivity can not be accomplished when RAM is present.

In summary, the sensitivity of laser FM spectroscopy is considerably reduced by the baseline and noise problems caused by the RAM. The detection limit is approximately

10^{-5} differential absorption,³³ 2 orders of magnitude worse than the quantum-limited sensitivity.

4. SAMPLE-DEPENDENT TECHNIQUES FOR OVERCOMING RESIDUAL AMPLITUDE MODULATION

Although complete elimination of the RAM is clearly the desirable goal, we will highlight here the results of several experiments that found other ways to circumvent the sensitivity limitations caused by the RAM. Most of these methods resorted to the more conventional sample-modulation techniques outlined in Section 1. The first report, to our knowledge, of quantum-limited detection sensitivity was published by Levenson *et al.*,³⁴ who used FM spectroscopy to measure the Raman gain in deuterium. By chopping the pump laser at a few kilohertz, these authors were able to achieve a shot-noise-limited sensitivity of 10^{-7} differential Raman gain. A similar approach was used in Ref. 35, where the technique of photochemical-modulation spectroscopy⁷ was combined with FM spectroscopy to achieve nearly shot-noise-limited, high-resolution absorption measurements of the formyl radical, HCO. This result is particularly significant as the HCO radical predissociates from the terminal level used for this measurement and is thus nearly impossible to detect by using fluorescence methods. The sensitivity was comparable with that achieved on the same radical using optogalvanic spectroscopy.³⁶

To understand how these sample-modulation methods improve achievable sensitivity, refer to Figures 5 and 6, which show the electronic power spectrum of the output of the mixer used to detect the FM signal in the photochemical modulation experiments. In these experiments the laser was mechanically chopped in addition to being frequency modulated. The chopping helped to eliminate a spurious pickup signal from the photochemical-modulation process. Figure 5 was taken in the absence of any photochemically modulated radicals and shows the laser fluctuation spectrum centered at the laser-chop frequency. This is the same leaked spectrum of Fig. 4 now brought back down in frequency by the rf mixer. In Fig. 6 the photochemical process by which the HCO radicals are formed has been switched on, and sidebands appear relative

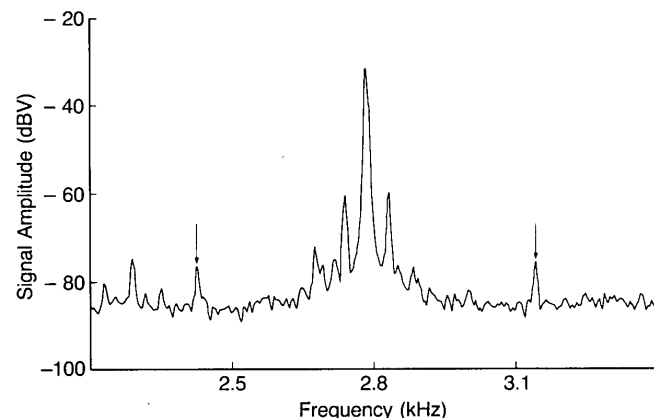


Fig. 6. Electronic power spectrum of the FM signal under the same conditions as in Fig. 5 except that now an absorbing sample of photochemically modulated HCO radicals is in the laser beam. The photochemical-modulation frequency is approximately 0.3 kHz, and the arrows in the figure point to the HCO-induced signals at 2.8 ± 0.3 kHz.

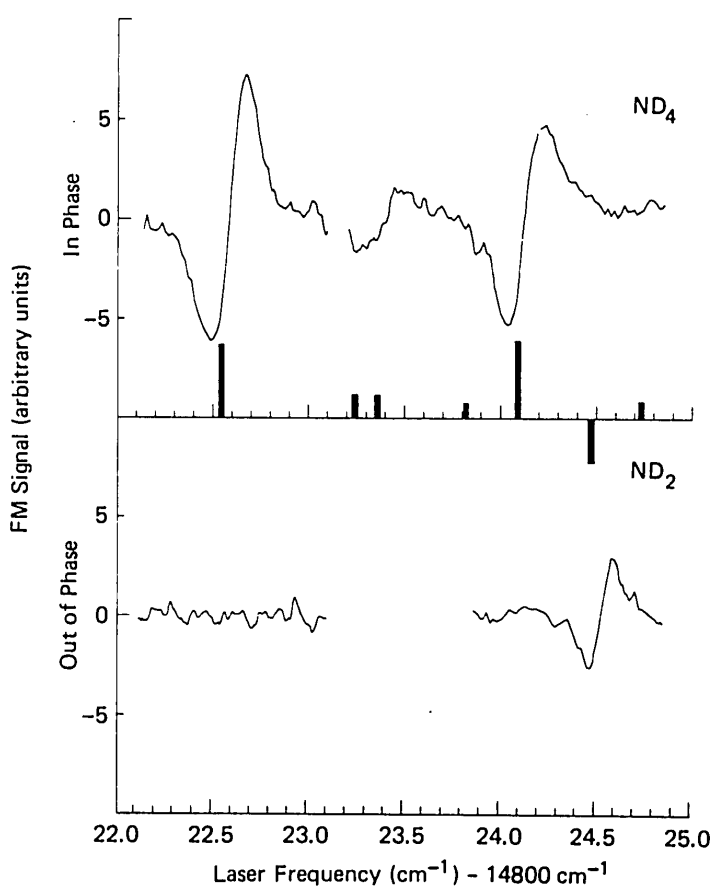


Fig. 7. Laser frequency scan showing the photochemical-modulation phase relationship between the ND_4 (upper part) and ND_2 (lower part) absorption signal. ND_2 is present as intermediate in the production of ND_4 . The markers show the location of the known transitions.³⁹ FM frequency, 2 GHz; laser-chop frequency, 2.8 kHz; photochemical-modulation frequency, 12 kHz. The signal was detected at 2.8 kHz + 12 kHz. The differential absorptivity for the ND_4 was approximately 10^{-5} .

to the RAM-induced peak of Fig. 5 shifted away from this peak by the photochemical-modulation frequency. These sidebands represent the FM signals of interest, and, as they appear in the wings of the RAM background, the sensitivity is increased by several orders of magnitude. All sample-modulation techniques operate in the same way.

The photochemical-modulation-FM-spectroscopy method was applied with great success to take the first absorption spectra of the ammonium radical ND_4 .³⁷ Figure 7 is a laser frequency scan through several lines of the ND_4 spectrum known previously from emission spectra.³⁸ The combination of the two methods permitted high-resolution, high-sensitivity measurements to be made on this radical and contributed to the discovery of a new photochemical pathway to its production. From the results of this experiment, it was argued that ND_4 is metastable in the ground state. This was later verified in Ref. 39.

Another important result using combined sample modulation and FM spectroscopy was reported by Jasinski *et al.*⁴⁰ These workers were able to detect by direct absorption the radical SiH_2 in modulated dc glow discharges of silane and disilane. SiH_2 is thought to play an important role in the decomposition of silane and disilane discharges used in chemical vapor deposition of amorphous silicon. Previous attempts to detect SiH_2 by laser-induced fluorescence and optogalvanic spectroscopy had been unsuccessful. Although

the chemical pathways important in these reactions are still not well understood, the authors report that FM spectroscopy will provide a useful new tool for *in situ* monitoring of chemical transients.

The last technique that we wish to highlight under sample-dependent methods of overcoming RAM uses quite a different approach than sample modulation. Romagnoli *et al.*⁴¹ report on the combination of polarization spectroscopy and FM spectroscopy to achieve significant gains in sensitivity. In this method, named FREMPOLSPCT, induced polarization anisotropies are used to upset the FM sideband balance. Though limited to samples in which such anisotropies are possible, the method has been used successfully to study persistent, anisotropic spectral holes in color centers of NaF and free-base phtalocyanine-doped polyethylene.⁴²

Taken together, these experiments illustrate the wide applicability of FM spectroscopy. Nonetheless, requiring sample modulation or anisotropy limits the range of systems that may be investigated. In Section 5 we discuss a new technique that permits the RAM background to be nulled, making possible quantum-limited detection of unmodulated, isotropic species.

5. A NEW, SAMPLE-INDEPENDENT DOUBLE-BEAM TECHNIQUE FOR SUPPRESSING RESIDUAL AMPLITUDE MODULATION

Recently, Gehrtz *et al.* proposed a simple double-beam, single-detector technique for nulling the RAM that is not subject to any restrictions.⁴³ Although related double-beam, single-detector schemes have been successfully used previously in WMS, they differ from the method used in Ref. 43 in some important aspects that will be pointed out below. In this section we will discuss the principles of this double-beam technique in full detail and present experimental evidence demonstrating the basic features predicted by the theory.

A. Outline of the Technique

The essentials of the double-beam technique are illustrated in Fig. 8. In the qualitative analysis that follows, it is assumed for the moment that no absorbing sample is present. With two beam splitters (BS's), a sample (*s*) and a reference (*r*) beam are generated and subsequently recombined onto the photodiode. A chopper (Ch) with a suitably large blade is used to chop both beams synchronously but 180° out of phase (cf. the insert in the upper left-hand corner of Fig. 8).⁴⁴ With both beams hitting the photodetector, therefore, the terms depending on ω_{chop} cancel (provided that the power levels in the two paths are made equal with a variable attenuator ND), and one is left with a dc signal at the mixer output. When the laser is scanned on a time scale slow compared with the chopper period, the final demodulation with the lock-in amplifier at ω_{chop} thus yields a zero baseline at the lock-in amplifier output.⁴⁵ It is important to emphasize here that the rf phases in the two beams have to be exactly equal in order for the proposed RAM nulling scheme to work at arbitrary modulation frequencies ω_{rf} . As is indicated in Fig. 8, this is easily achieved by equalizing the two beam path lengths l_s and l_r . Note that this adjustment has to be accomplished only with an accuracy given by the rf wavelength, i.e., on a scale of several centimeters to several meters for the modulation frequencies generally used in our experiments. Consequently,

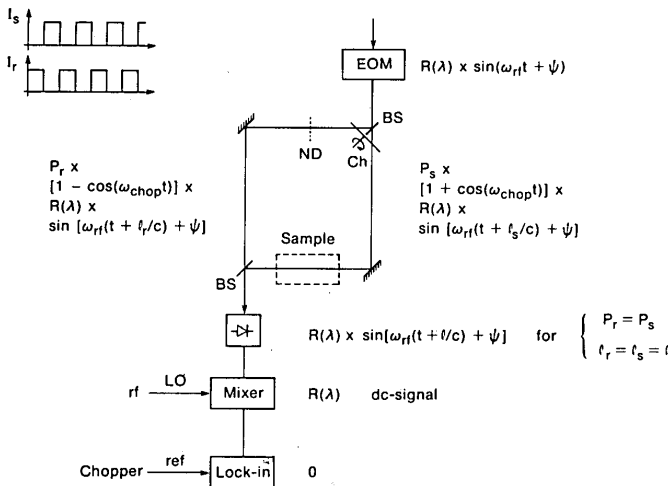


Fig. 8. Schematics illustrating the double-beam, one-detector RAM-nulling technique. $R(\lambda)$ represents the modulation index of the RAM, and ψ is the phase shift between the FM and the RAM.^{24,25} Unimportant constant factors are omitted here for brevity. With two beam splitters (BS's), a sample (s) and a reference (r) beam are generated and subsequently recombined onto the photodiode. A chopper (Ch) serves to chop both beams synchronously but 180° out of phase (cf. the insert in the upper left-hand corner of the figure). With both beams hitting the photodetector, the terms depending on the chopper frequency ω_{chop} cancel one another (provided the relative power levels P_s and P_r in the two paths are made equal with a variable attenuator ND, and the path lengths l_s and l_r are equalized). One is left, finally, with a dc signal at the mixer output. In effect this technique shifts the unwanted RAM signal out of the frequency band of interest at ω_{chop} to zero frequency.

it is relatively straightforward to account for this path-length requirement once and for all when the double-beam setup is built—under regular environmental conditions, no active control of the path lengths is necessary for proper operation of the double-beam technique.

We now proceed to an outline of the general case when an absorbing sample is present in the s beam: Although the reference beam carries the no-sample background signal $I_{ns}(t)$ [Eq. (3.12)]:

$$I_r(t) = P_r I_{ns}(t) (1 - \cos \omega_{\text{chop}} t), \quad (5.1)$$

the sample beam carries the complete signal $I(t)$ [Eq. (3.11)]:

$$I_s(t) = P_s(t) (1 + \cos \omega_{\text{chop}} t). \quad (5.2)$$

In fact, the intensities $I_r(t)$ and $I_s(t)$ also contain terms depending on higher harmonics of the chopper frequency ω_{chop} . These terms are effectively rejected by the lock-in amplifier, which is synchronized to the fundamental of ω_{chop} , and are thus discarded here for brevity. Note the opposite signs of the cosine terms corresponding to the 180° phase shift between the two beam intensities. The dimensionless quantities $P_{r,s}$ denote the relative light power in the two beams.

The beams are subsequently recombined on the photodiode, and the two beam path lengths are equilized as discussed above:

$$l_r = l_s. \quad (5.3)$$

Provided that the power in the reference beam is adjusted such that

$$P_r = \exp(-2\delta) P_s, \quad (5.4)$$

the total intensity impinging on the photodiode is (cf. Subsection 3.A)

$$I_{\text{tot}}(t) = P_r [I_0 + 2B(t)] + P_s F(t)(1 + \cos \omega_{\text{chop}} t). \quad (5.5)$$

Note that the pure-FM signal $F(t)$ [Eq. (2.9)] is labeled by the additional modulation term depending on the chopper frequency ω_{chop} , whereas the background signal $B(t)$ [Eq. (3.10)] does not contain ω_{chop} . The mixer output is proportional to

$$M_{\text{tot}}(\lambda) = 2P_r \hat{B}(\lambda) + P_s \hat{F}(\lambda)(1 + \cos \omega_{\text{chop}} t). \quad (5.6)$$

The double-beam technique therefore effectively shifts the unwanted background signal $\hat{B}(\lambda)$ [Eq. (3.15)] to zero frequency, leaving the FM signal $\hat{F}(\lambda)$ [Eq. (2.11)] at the chopper frequency. After the mixer output is demodulated with a lock-in amplifier,⁴⁵ the total signal is proportional to

$$L_{\text{tot}}(\lambda) = P_s \hat{F}(\lambda), \quad (5.7)$$

and, in the absence of any absorbing sample (subscript ns), one indeed obtains a zero background

$$L_{\text{tot},\text{ns}}(\lambda) = 0. \quad (5.8)$$

Before we proceed to the experimental demonstration of the double-beam RAM-suppression scheme, the double-beam technique is further analyzed from a different point of view in Fig. 9, emphasizing the sequential demodulation steps involved. In particular, this analysis shows that when the powers in the two beams are properly adjusted [Eq. (5.4) with

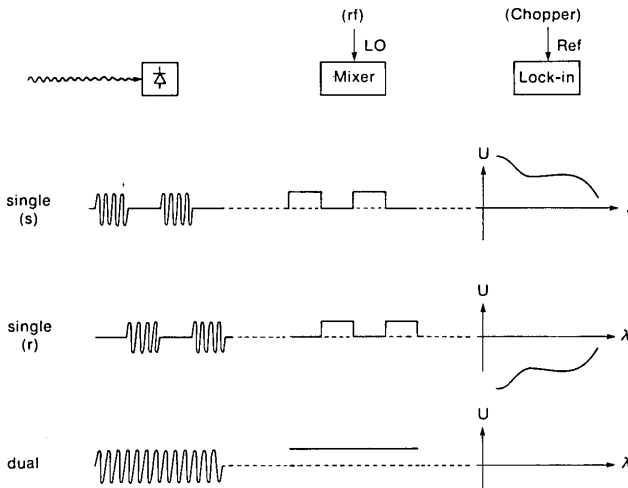


Fig. 9. Schematic diagram showing the sequential steps involved in demodulating the RAM-induced photosignal; first, for each of the beams separately (single s and r) and then for the actual double-beam case (dual). Because each of the individual beams is chopped and carries the RAM signal $B(t)$ [cf. Eqs. (3.10) and (3.12)] one obtains rf bursts at the chopper frequency even when no sample is present. After the first demodulation with the mixer, these rf bursts are converted into a square-wave signal, which is subsequently demodulated at the chopper frequency with a lock-in amplifier yielding a dc-output signal. Now, when the laser is scanned slowly (on the time scale of the chopper period), one finally obtains an output voltage $U(\lambda)$, which is proportional to $P_s \hat{B}(\lambda)$ when the reference beam path is blocked, i.e., when only the sample beam is used. Correspondingly, the output voltage for the reference beam only is proportional to $-P_r \hat{B}(\lambda)$. Finally, both beams are allowed to impinge on the photodetector (dual), and one obtains a continuous-wave rf output signal that, after demodulation with the mixer, converts to a dc-signal. As this signal has no frequency components at the chopper frequency, the final demodulation with the lock-in amplifier yields a zero output voltage [i.e., $L_{\text{tot},\text{ns}}(\lambda)$ in Eq. (5.8)].

$\bar{\delta} = 0$] the lock-in amplifier output voltages corresponding to the two individual beams are exactly equal but have opposite sign:

$$L_{s,ns}(\lambda) = -L_{r,ns}(\lambda). \quad (5.9)$$

The validity of this relation will be experimentally demonstrated below.

B. Demonstration of the Basic Features

A full account of the FM-spectroscopy apparatus will be given in Section 6. Here we focus on the double-beam, single-detector setup. Several implementations have been tested that differ mainly in the double-beam-generation part. Using a chopper with mirrored blades instead of a beam splitter followed by an absorbing chopper (as is shown in Fig. 8) has the advantage of actually using nearly all the light power emerging from the EOM. The directional instability of the reflected beam, however, poses a serious disadvantage. Using a galvodriven mirror (General Scanning GP 300 series) to switch the beam between two directions into the sample and the reference path did not allow for sufficiently high switching rates ($v_{switch} \leq 60$ Hz).

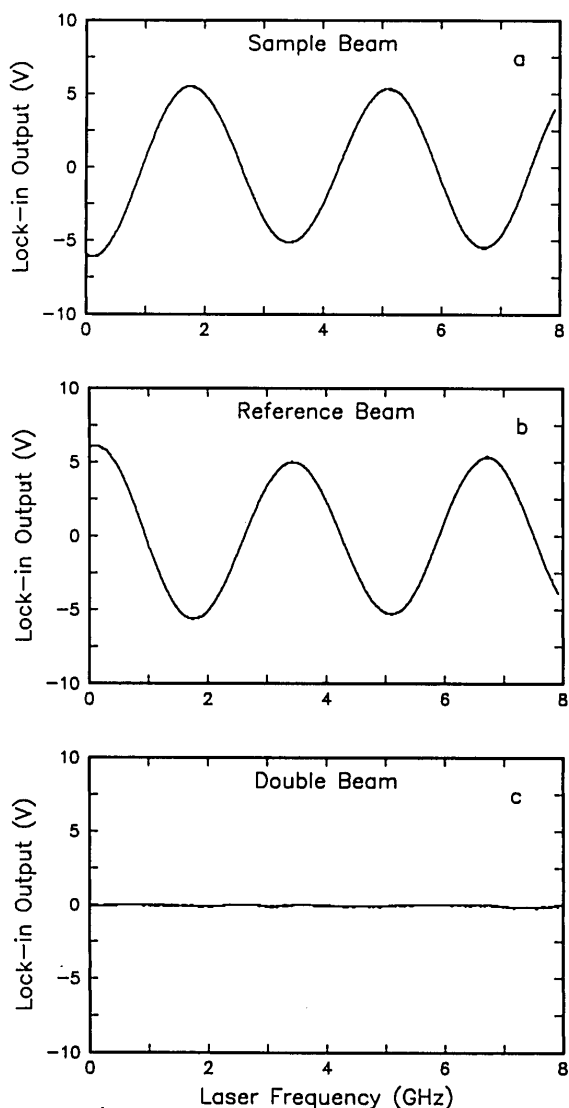


Fig. 10. Demonstration of the basic features of the double-beam technique. The RAM fringe traces obtained with a, the sample and b, the reference beam separately have opposite sign as required by Eq. (5.9). With both beams impinging on the photodetector (trace c) the RAM fringes are efficiently suppressed [Eq. (5.8)].

In order to get high switching rates, an acousto-optic modulator (AOM) was tried. An Isomet 1206-1 modulator was driven with an isomet 323 driver. By gating the AM input of the driver high and feeding a square wave with $v_{switch} = 10$ kHz into the voltage-control oscillator input of the driver, the AOM is alternately driven by $v_{low} = 81$ MHz and $v_{high} = 132$ MHz. Consequently, the beam is switched between two deflection angles and directed into the sample-and the reference-beam path at the required phase shift of 180° . Note that the zero-order (nondeflected) beam is not used in this configuration in order to avoid problems associated with the limited contrast generally observed in zero order. With the AOM-generated double-beam, single-detector setup, the RAM could be suppressed by a factor of more than 150. Our preliminary experiments showed, however, that this implementation is not suitable for achieving quantum-limited performance in laser FM spectroscopy, mainly because of apparent additional rf phase shifts experienced by the two beams as they traverse the AOM. Although the EOM driver frequency was carefully chosen not to be an integer multiple of one of the AOM driver frequencies, all these frequencies are still of the same order of magnitude. It is thus conceivable that the AOM affects the rf phase behavior of the FM laser beam, and it does so differently for the sample and the reference beams. The exact interaction of an AOM with a FM laser beam is not known at present; we are puzzled by the fact that the apparent rf phase-shift difference imposed on the two beams changes drastically when the laser beam path through the AOM crystal is changed slightly (on a submillimeter scale).

The most reliable implementation is the (absorptive) chopper-generated double-beam configuration, as shown schematically in Fig. 8. In practice, the chopper was placed after the sample to avoid possible problems with potentially slow kinetics of the sample absorption. In order to use all the light power contained in the sample and the reference beams, a first surface mirror in conjunction with a short-focal-length lens was used as beam-recombination optics instead of a second beam splitter. This double-beam configuration was employed for the quantum-limited FM-spectroscopy experiments described in Section 6. Here we want to demonstrate briefly the basic features of the double-beam technique that are expressed in Eqs. (5.8) and (5.9). With no sample in the beam, the setup was aligned according to the path length [Eq. (5.3)] and the power requirement [Eq. (5.4) with $\bar{\delta} = 0$]. The laser is scanned over 8 GHz. The single-beam spectra in Figs. 10a and 10b are obtained by blocking the reference and the sample beam, respectively. The fringes are due to the EOM, which is deliberately set in a multipass configuration (cf. Subsection 3.B). The fringe traces obtained with the sample and the reference beam separately have opposite sign and demonstrate the validity of Eq. (5.9). Now, when both beams are unblocked, the RAM fringes are suppressed efficiently (Fig. 10c). The weak spurious fringes on the suppressed RAM trace are probably due to étalon effects occurring in only one of the beams.

6. QUANTUM-LIMITED LASER FREQUENCY-MODULATION SPECTROSCOPY

With the double-beam, single-detector scheme described in the previous section, quantum-limited detection of an un-

modulated, isotropic spectral feature with laser FM spectroscopy was demonstrated for the first time, to our knowledge, in Ref. 43. In this section we demonstrate the limitations to the sensitivity of laser FM spectroscopy caused by the RAM and show how these limitations can be readily overcome and shot-noise-limited sensitivity achieved with the double-beam technique. For the sake of reference, the experimental apparatus is described in full detail here.

A. Experimental Setup

The apparatus employed in the experiments is as follows (Figs. 1 and 8): The tunable dye laser is a Coherent 699-21 ring laser pumped by a Spectra-Physics 171 argon-ion laser. The EOM, a Lasermetrics 1039C AD*P modulator, is driven at 249 MHz by a Hewlett-Packard 8640A signal generator amplified to 1-W average power with an ENI 603L power amplifier. The beam is then sent through the double-beam setup (Fig. 9) and detected by a EG&G FND-100 photodiode. The photodiode output is filtered with a K&L 200-MHz high-pass filter, amplified with a Q-Bit QB-538 rf amplifier, and mixed in a Minicircuits Laboratories ZFM-4 double-balanced mixer, with a LO derived from the signal generator. The mixer output is low-pass filtered and amplified in a home-made postmixer preamplifier (PMPA)³⁴ and directed to an Ithaco 393 lock-in amplifier synchronized to the chopper (operated typically at 1.65 kHz). The 100-Hz bandwidth of the lock-in amplifier determines the overall bandwidth of the detection system. The spectra are recorded with a Tektronix 7D20 digitizer and averaged to reduce the effective-noise bandwidth further to the values that we quote below.

The spectra were taken with the dye laser tuned to 569.746 nm and scanned over 8 GHz. The absorbing sample was iodine vapor in a 20-cm cell whose vapor pressure was controlled by cooling a sidearm of the cell with a dry-ice-methanol mixture (with the detection volume maintained at room temperature). The FM-signal voltage versus absorptivity calibration^{29,35} was done with the sidearm at 0°C [corresponding to a vapor pressure of 31 mTorr (Ref. 46)] so that the peak absorptivities could be determined directly from a transmission spectrum.

B. Elimination of Baseline Problems with the Double-Beam Setup

The sensitivity limitations that are due to the RAM-induced nonzero baseline and the performance of the RAM-suppression technique are demonstrated in Figs. 11 and 12. Here, we compare spectra obtained with the double-beam setup (Figs. 11b and 12b and 12d) with spectra recorded with the reference beam blocked (Figs. 11a and 12a and 12c), which corresponds to the conventional single-beam FM configuration. By cooling the iodine-cell sidearm to temperatures below -40°C, iodine-vapor pressures in the μ Torr regime are obtained,⁴⁶ and the absorptivities (which are proportional to the iodine-molecule number density) of the spectral lines studied decrease correspondingly.

The EOM is first set deliberately in a multipass configuration, which results in the strongly laser wavelength-dependent fringe RAM (cf. Subsection 3.B). Figure 11a shows the spectrum obtained with the sample beam only (the reference beam is blocked). The iodine-vapor pressure is set as high as 230 μ Torr, but the iodine FM signals are virtually buried in the strongly varying fringe-RAM baseline. In Fig.

11b the reference beam is unblocked, and the lock-in amplifier sensitivity is increased by a factor of 10. Note that, in contrast to Fig. 10, we here refer the FM signals to the (amplified) mixer output in order to account for necessary changes in lock-in amplifier sensitivity. The double-beam spectrum clearly demonstrates the capability of the new technique to recover even weak FM signals that would be barely detectable using the conventional single-beam FM setup.

The EOM is next angled with respect to the input laser beam, and one is left with the single-pass RAM (cf. Subsection 3.B). The iodine-vapor pressure can now be reduced further

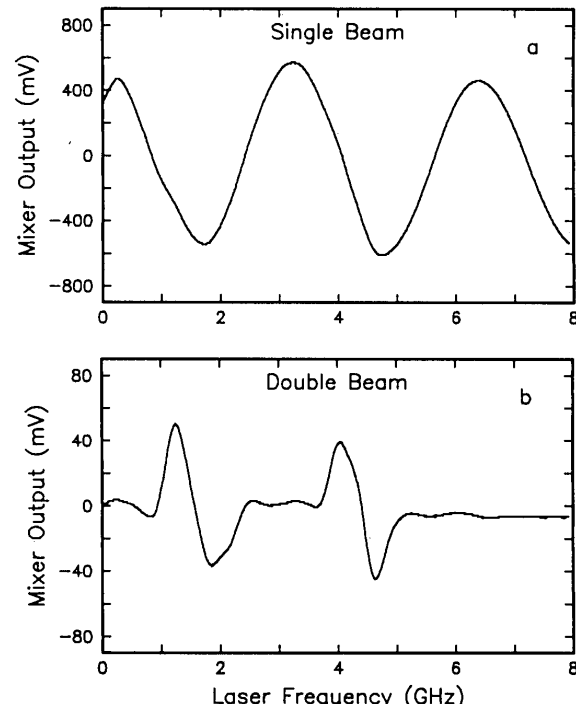


Fig. 11. FM spectra obtained with an iodine absorption cell, demonstrating the sensitivity limitations due to a, multipass RAM fringes and b, the efficient RAM nulling with the double-beam technique. Note the 10-times-increased sensitivity in b. The iodine-vapor pressure was 230 μ Torr.

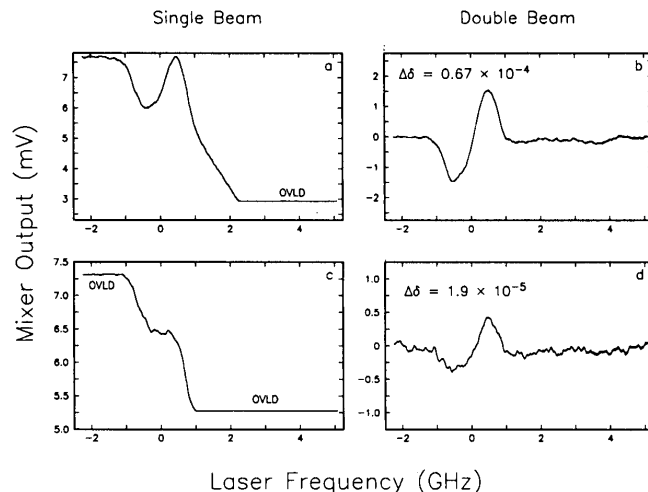


Fig. 12. FM spectra obtained with an iodine absorption cell, demonstrating the sensitivity limitations that are due to single-pass RAM (a and c) and the efficient RAM nulling with the double-beam technique (b and d). The lock-in amplifier starts to overload (OVLD) in the single-beam recordings. The modulation index used was 0.047, and the effective-noise bandwidth was 12.5 Hz. The iodine-vapor pressure was 33 μ Torr for traces a and b and 10 μ Torr for traces c and d.

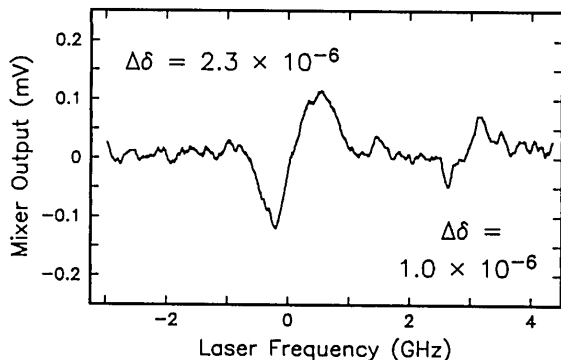


Fig. 13. FM spectrum of weak iodine absorption lines, obtained with the double-beam technique, demonstrating shot-noise-limited sensitivity. The modulation index used was 0.11, and the effective noise bandwidth was 1 Hz. The iodine-vapor pressure was $1.6 \mu\text{Torr}$. The frequency scale (abscissa) is offset by 17771.48 cm^{-1} .

by approximately 1 order of magnitude before the RAM-induced baseline problems become appreciable. In the single-beam spectrum in Fig. 12a (obtained at an iodine-vapor pressure of $33 \mu\text{Torr}$) the FM signal is strongly distorted, rendering difficult, e.g., attempts to measure quantitatively the absorptivity at this vapor pressure. At a pressure of $10 \mu\text{Torr}$ (Fig. 12c) the iodine signal is completely buried in the sloping baseline. Note that this limitation can neither be overcome by increasing the EOM driving power (thus increasing the modulation index) nor by narrowing the effective-noise bandwidth of the detection system.

With the double-beam technique, the sensitivity limitations that are due to RAM are readily overcome, as is shown in Figs. 12b and 12d. Note the zero baseline of these signals as compared with the large offset of the corresponding single-beam spectra. The absorptivities⁴⁷ obtained from the FM spectra (indicated in Figs. 12b and 12d) are in excellent agreement with the corresponding values calculated independently from the iodine-molecule number densities (obtained from the sample-cell sidearm temperatures and using published⁴⁶ iodine-vapor pressure data):

$$\Delta\delta_{\text{calc}}^{\text{b}} = 0.63 \times 10^{-4} \quad \text{and} \quad \Delta\delta_{\text{calc}}^{\text{d}} = 1.97 \times 10^{-5}.$$

C. Quantum-Limited Sensitivity with the Double-Beam Setup

In order to demonstrate the full capability of the double-beam, one-detector FM scheme; we increased the modulation index and narrowed the effective-noise bandwidth (Fig. 13). The laser was tuned to a pair of adjacent iodine absorption lines, and the FM signals were again calibrated against a direct-transmission spectrum obtained at a sidearm temperature of 0°C corresponding to a vapor pressure of 31 mTorr . The pressure was then decreased to $(1.6 \pm 0.1) \mu\text{Torr}$ by cooling the sidearm to $(-71.5 \pm 0.5)^\circ\text{C}$. The absorptivities⁴⁸ obtained from the FM signals (which are indicated in Fig. 13) are in good agreement with the corresponding values calculated from the vapor-pressure reduction. The SNR's of the two FM signals are 13 and 6, implying a detection limit of $0.1 \mu\text{Torr}$ or

$$\Delta\delta_{\text{min}}(\text{exp}) = 1.7 \times 10^{-7}.$$

This has to be compared with the theoretical detection limit predicted from the SNR analysis in Ref. 28. Using the overall

light intensity (sample and reference beam) Eq. (2.12) yields

$$\Delta\delta_{\text{min}}(\text{calc}) = 1.9 \times 10^{-7}.$$

In view of the uncertainties, e.g., in measuring the modulation index, this is in excellent agreement with the experimental value shown above, indicating that we have in fact achieved shot-noise-limited sensitivity in this experiment. In the following subsection we discuss the noise reduction achieved with the double-beam technique and present further evidence for its quantum-limited performance.

D. Noise Reduction with the Double-Beam Setup

Although an increase in the SNR was expected with the double-beam technique as compared with the conventional single-beam setup, it is hard to make a quantitative assessment from the FM spectra in Fig. 12. Thus a series of careful measurements with an electronic spectrum analyzer (Hewlett-Packard 3582A) was performed in order to determine the low-frequency power spectrum at the mixer output. The sample cell was removed from the setup for these experiments. The spectra in Fig. 14 clearly demonstrate the capability of the double-beam method to suppress, along with the RAM, the low-frequency noise feedthrough associated with it (cf. Subsection 3.C). In the single-beam spectrum (Fig. 14a, upper curve) of the amplifier mixer output after the PMPA, the RAM manifests itself as a peak at the 1650-Hz chopper frequency accompanied by two noise sidebands displaced by $\pm 60 \text{ Hz}$.⁴⁹ The corresponding low-frequency spectrum of the direct photodiode output (now shown here) reveals that these sidebands constitute the feedthrough of the strongest components in the low-frequency noise spectrum of the dye-laser output, shifted to the detection frequency ($\omega_{\text{rf}} + \omega_{\text{chop}})/2\pi$). The noise sidebands are fully suppressed below the shot-noise level in the double-beam spectrum (Fig. 14b, upper curve) along with the RAM signal proper, which is diminished by more than 40 dB.

Note the difference from the sample-modulation method highlighted in Fig. 6: There the interfering RAM signal is left unchanged, and one relies on sample modulation to shift the FM signal under study away from the RAM-induced noise spectrum. With the double-beam technique, on the other hand, the RAM signal itself is moved out of the detection frequency band of interest, and one obtains a shot-noise-limited condition in this band.

Great care was taken to ensure that the dominant noise

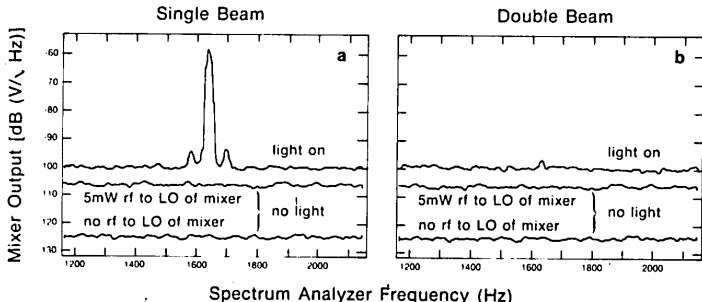


Fig. 14. Power spectra of the amplified mixer output (after the PMPA), showing RAM peaking at the chopper frequency and associated low-frequency noise feedthrough with a, the single-beam technique, and their suppression with b, the double-beam technique. No sample was in the s-beam path. The light levels were the same for both light-on spectra (16 mW).

source is in fact shot noise. (1) The noise spectrum is light dependent with the expected power dependence ($\propto \sqrt{I_0}$). Neither the PMPA noise nor the signal-analyzer noise dominates the no-light noise spectra (as is indicated by the bottom spectra in Fig. 14). (2) The observed light-on and no-light noise levels (upper and middle curves in Fig. 14) are in excellent agreement with the calculated shot-noise and Johnson-noise levels, respectively. They do not change when the rf power to the EOM is switched off (whereas the RAM peak and the 60-Hz sidebands shown in Fig. 14a disappear, of course), indicating negligible rf pickup. (3) Finally, the high-frequency noise spectrum of the (amplified) photodiode signal itself was determined with a Hewlett-Packard 8568B spectrum analyzer and was found to be flat around the modulation frequency chosen for our experiments, indicating that excess noise caused by pump-laser-mode beats does not interfere with our measurements.

7. APPLICATIONS

The combination of high sensitivity and high resolution renders FM spectroscopy an attractive tool in many application areas. Of particular future interest might be remote or non-contact trace-gas detection in combustion, flame, or plasma diagnostics or in environmental-pollution control. In fact, the FM-spectroscopy technique has been proposed for improved detection of OH,⁵⁰ and FM spectroscopy with a CO₂ laser has been considered for long-path measurement of hydrazine fuel gases.⁵¹ The peculiarities of conducting FM spectroscopy in the far infrared (with a CO₂ laser) have been investigated by Cooper *et al.*⁵²

Recently, a series of experiments has been started in our laboratory, which demonstrate for the first time, to our knowledge, the use of FM spectroscopy in ultrasensitive detection of an important air-pollution constituent. For a variety of reasons, we chose NO₂ for these experiments. NO₂ is recognized as one of the major air pollutants^{53,54}. In addition to its direct toxicity, it is involved in many chemical reactions in the troposphere,⁵⁵ which can lead to the formation of photochemical smog, and, when washed out by rain, substantially contributes to the acidification problem. NO₂ has a wealth of narrow absorption lines in the visible⁵⁶ and in the near infrared.⁵⁷

The measurements using the visible absorption lines were performed with the same apparatus described previously (Subsection 6.A). A Burleigh WA-10 wavemeter was employed to set the dye laser to a spectral region of the NO₂ absorption spectrum, where adjacent lines would not overlap and could be compared with published NO₂ spectral data.⁵⁶ In one set of experiments the dye laser was tuned to 571.722 nm (vacuum wavelength) and scanned over 8 GHz. With the wavemeter, the NO₂ absorption lines at 17490.94 and 17491.09 cm⁻¹ (vacuum wave numbers, cf. Ref. 56, p. 187) could be readily identified. The NO₂ gas was contained in a 25-cm cell with Brewster-window end pieces that was evacuated previous to the experiments. A sidearm of the cell contained the NO₂-N₂O₄ equilibrium mixture corresponding to the temperature of the sidearm cooling bath.⁴⁶ The NO₂ partial pressure was set to 1 Torr, and the FM signals obtained here were used for calibrating the signals recorded subsequently. The absorption lines studied quantitatively have differential amplitude absorptivities of 0.45 m⁻¹ and 0.63 m⁻¹, respec-

tively. The sidearm was then shut off, and the sample cell was pumped down slowly. As pressure-broadening effects are likely to be absent under these low-pressure conditions, we assume a linear relationship between the FM-signal peak-peak voltages and the NO₂ partial pressure in the cell. Note that this assumption has been confirmed for the iodine-detection experiments described in Section 6.

From these experiments we infer a detection limit [or noise-equivalent partial pressure (NEPP)] of

$$\text{NEPP} \sim 0.7 \frac{\mu\text{Torr}}{\text{m (path length)}}$$

when a 1-Hz detection bandwidth and a FM index of $M = 0.1$ is employed. This NEPP would scale inversely with the square root of the detection bandwidth. This is to be contrasted with the detection limit set by RAM when the conventional single-beam setup is used. This RAM-equivalent partial pressure (REPP) is limited not by the bandwidth but by the RAM-induced background:

$$\text{REPP} \sim 1000 \frac{\mu\text{Torr}}{\text{m (path length)}}.$$

The 3-orders-of-magnitude improvement observed here again demonstrates the excellent performance of the double-beam, single-detector FM-spectroscopy technique. Further work is necessary, however, to evaluate the sensitivity limits in NO₂ detection under realistic environmental conditions, e.g., under foreign-gas pressure, where pressure broadening starts to affect the line shapes of the absorption lines.

The near-infrared absorption lines of NO₂ fall mostly into the regime of GaAlAs-laser emission; e.g., the (000) \leftarrow (000) vibronic bandhead of the $^2B_2 \leftarrow ^2A_1$ electronic transition is at 836.5 nm.⁵⁷ GaAlAs lasers are particularly attractive for laser FM-spectroscopy applications, mainly because they are low-cost devices that can be easily frequency modulated by directly modulating the injection current. Thus no external modulators are necessary. High-frequency heterodyne spectroscopy with GaAlAs lasers has been demonstrated recently,^{24,25} and it was found that for moderate sensitivity requirements the fairly strong RAM invariably associated with injection-current modulation poses no problem in GaAlAs-laser FM spectroscopy.

Quantum-limited performance of semiconductor-laser FM spectroscopy, however, has not yet been demonstrated. Recent preliminary experiments in our laboratory indicate that noise and baseline problems associated with the RAM cause a NO₂ near-infrared detection limit of approximately 1 mTorr/m (path length). Further work is now in progress to solve the RAM problem in GaAlAs-laser FM spectroscopy and to achieve quantum-limited performance.

8. SUMMARY

Laser FM spectroscopy combines the advantages of direct-absorption techniques with the high resolution achievable with lasers and the high sensitivity of modulation techniques. In principle, shot-noise-limited detection sensitivity should be possible with FM spectroscopy. In practice, however, the sensitivity is limited by the inevitable RAM to values 2 to 3 orders of magnitude worse than the quantum limit. A variety of techniques has been developed in order to overcome this limitation. All these methods rely on specific properties of

the sample: They require either that the sample absorption (or gain) be modulated or that the sample absorption be anisotropic.

The new double-beam, single-detector technique that is described in some detail here permits the sensitivity limitations caused by the RAM to be overcome without any restrictions to the sample under study. Specifically, the RAM-induced, nonzero baseline is reduced by more than 40 dB, and the RAM-induced low-frequency noise feedthrough is fully suppressed below the shot-noise level. With this double-beam technique, quantum-limited performance of laser FM spectroscopy on unmodulated, isotropic spectral features was demonstrated for the first time to our knowledge.

This improved FM technique is an attractive tool for high-sensitivity, high-resolution trace-gas detection, e.g., in air-pollution control. In preliminary experiments with NO₂, a detection limit in the sub- μ torr regime was achieved.

ACKNOWLEDGMENT

The authors would like to thank M. D. Levenson and W. Lenth for valuable discussions.

* IBM World Trade Visiting Scientist on leave from the Institut für Physikalische Chemie der Universität München, Federal Republic of Germany.

REFERENCES

- G. C. Bjorklund, IBM Invention Disclosure SA 8790135 (March 1979); "Frequency-modulation spectroscopy: a new method for measuring weak absorptions and dispersions," *Opt. Lett.* **5**, 15 (1980); U.S. Patent 4,297,035 (November 1981).
- The FM technique was independently suggested by R. W. P. Drever as a means for servolocking a tunable laser to a high-finesse optical cavity. It was first experimentally implemented for this purpose by R. W. P. Drever, J. L. Hall, F. V. Kowalski, J. Hough, G. M. Ford, and A. J. Munley, Joint Institute for Laboratory Astrophysics, Boulder, Colo. 80303 (personal communication, September 1979) and then by M. Prentiss, B. Peuse, G. Sanders, S. Ezekiel, Research Laboratory of Electronics, Progress Rep. No. 123 (Massachusetts Institute of Technology, Cambridge, Mass., January 1981).
- The most recent applications of FM spectroscopy are described in Refs. 35, 37, and 40. For a review of the use of FM techniques covering the literature up to 1983, cf. Ref. 28 and references therein.
- N. Nayak and G. S. Agarwal, "Absorption and fluorescence in frequency-modulated fields under conditions of strong modulation and absorption," *Phys. Rev. A* (to be published).
- N. H. Tran, R. Kachru, P. Pillet, H. B. van Linden van den Heuvell, T. F. Gallagher, and J. P. Watjen, "Frequency-modulation spectroscopy with a pulsed dye laser: experimental investigations of sensitivity and useful features," *Appl. Opt.* **23**, 1353 (1984).
- D. E. Cooper and T. F. Gallagher, "Frequency-modulation spectroscopy with a multimode laser," *Opt. Lett.* **9**, 451 (1984).
- H. E. Hunziker, "A new technique for gas-phase kinetic spectroscopy of molecules in the triplet state," *IBM J. Res. Develop.* **15**, 10 (1971).
- M. Cardona, *Modulation Spectroscopy*, Supplement II of Solid State Physics, F. Seitz and D. Turnbull, eds. (Academic, New York, 1969).
- C. S. Gudemann, C. C. Marner, M. H. Begemann, E. Schafer, J. Pfaff, and R. J. Saykally, "Velocity modulation laser absorption spectroscopy of molecular ions," *Proc. Soc. Photo-Opt. Instrum. Eng.* **426**, 106 (1983).
- J. L. Hall, T. Baer, L. Hollberg, and H. G. Robinson, "Precision spectroscopy and laser frequency control using FM sideband optical heterodyne techniques," in *Laser Spectroscopy V*, A. R. W. McKellar, T. Oka, and B. P. Stoicheff, eds. (Springer-Verlag, Berlin, 1981), p. 16.
- M. Ducloy and J. J. Snyder, "High frequency optical heterodyne spectroscopy," *Proc. Soc. Photo-Opt. Instrum. Eng.* **426**, 87 (1983).
- A. L. Huston and W. E. Moerner, "Detection of persistent spectral holes using ultrasonic modulation," *J. Opt. Soc. Am. B* **1**, 349 (1984).
- A. L. Huston and W. E. Moerner, IBM Research Laboratories, San José, Calif. 95193 (personal communication).
- E. I. Moses and C. L. Tang, High-sensitivity laser wavelength-modulation spectroscopy, *Opt. Lett.* **1**, 115 (1977).
- P. Pokrowsky, W. Zapka, F. Chu, and G. C. Bjorklund, "High frequency wavelength modulation spectroscopy with diode lasers," *Opt. Commun.* **44**, 175 (1983).
- D. S. Klier, ed., *Ultrasensitive Laser Spectroscopy* (Academic, New York, 1983).
- J. A. Gelbwachs, C. F. Klein, and J. E. Wessel, "Saturated optical nonresonant emission spectroscopy (SONRES) for atomic detection," *Appl. Phys. Lett.* **30**, 489 (1977).
- J. Allen, W. R. Anderson, and D. Crosley, "Optoacoustic pulses in a flame," *Opt. Lett.* **1**, 118 (1977).
- P. K. Schenk and J. W. Hastie, "Optogalvanic spectroscopy—application for combustion systems," *Opt. Eng.* **20**, 522 (1981).
- T. D. Harris and A. M. Williams, "Low absorbance measurements," *Proc. Soc. Photo-Opt. Instrum. Eng.* **426**, 110 (1983).
- T. Hirschfelder, "The choice between absorption and fluorescent techniques," *Appl. Spectrosc.* **31**, 245 (1977).
- J. D. Ingle, Jr., "Additional comments relating to the choice between absorption and fluorescent techniques," *Appl. Spectrosc.* **36**, 588 (1982).
- G. C. Bjorklund, W. Lenth, and C. Ortiz, "Cryogenic frequency domain optical mass memory," *Proc. Soc. Photo-Opt. Instrum. Eng.* **298**, 107 (1982).
- W. Lenth, "Optical heterodyne spectroscopy with frequency- and amplitude-modulated semiconductor lasers," *Opt. Lett.* **8**, 575 (1983).
- W. Lenth, "High frequency heterodyne spectroscopy with current-modulated diode lasers," *IEEE J. Quantum Electron.* **QE-20**, 1045 (1984).
- A. Yariv, *Quantum Electronics*, 2nd ed. (Wiley, New York, 1975), pp. 341–343.
- J. L. Hall, H. G. Robinson, T. Baer, and L. Hollberg, "The line-shapes of subdoppler resonances observable with FM side-band (optical heterodyne) laser techniques," in *Advances in Laser Spectroscopy*, F. T. Arecchi, F. Strumia, and H. Walther, eds. (Plenum, New York, 1983), p. 99.
- G. C. Bjorklund, M. D. Levenson, W. Lenth, and C. Ortiz, "Frequency modulation (FM) spectroscopy—theory of lineshapes and signal-to-noise analysis," *Appl. Phys. B* **32**, 145 (1983).
- E. A. Whittaker, P. Pokrowsky, W. Zapka, K. Roche, and G. C. Bjorklund, "Improved laser technique for high sensitivity atomic absorption spectroscopy in flames," *J. Quantum. Spectrosc. Radiat. Transfer* **30**, 289 (1983).
- L. Hollberg, Ma Long-sheng, M. Hohenstatt, and J. L. Hall, "Precision measurements by optical heterodyne techniques," *Proc. Soc. Photo-Opt. Instrum. Eng.* **426**, 91 (1983).
- When current modulated diode lasers are used for FM spectroscopy,^{24,25} one generally has to deal with a fairly strong RAM ($R/M \sim 0.1$). It was recognized in Refs. 24 and 25, however, that the RAM phase difference ψ depends critically on the diode-laser operating conditions. It should thus be possible to set ψ such that the distortive term becomes small compared with the pure-FM term—at least for the Fourier component being studied (in phase or quadrature).
- E. A. Whittaker, M. Gehrtz, and G. C. Bjorklund, "Residual amplitude modulation in laser electro-optic phase modulation," *J. Opt. Soc. Am. B* **2**, 1320–1326 (1985).
- A possible improvement on this situation has been reported by B. A. Woody and L. Lyndz (Appl. Opt., to be published) who report a sensitivity limit of $\sim 10^{-6}$. We thank the authors for a personal communication of their preliminary results.
- M. D. Levenson, W. E. Moerner, and D. E. Horne, "FM spec-

- troscopy detection of stimulated Raman gain," *Opt. Lett.* **8**, 108 (1983).
35. E. A. Whittaker, H. R. Wendt, H. E. Hunziker, and G. C. Bjorklund, "Laser FM spectroscopy with photochemical modulation: a sensitive, high resolution technique for chemical intermediates," *Appl. Phys. B* **35**, 105 (1984).
 36. R. Vasudev and R. N. Zare, "Laser optogalvanic study of HCO A state predissociation," *J. Chem. Phys.* **76**, 5267 (1982).
 37. E. A. Whittaker, B. J. Sullivan, G. C. Bjorklund, H. R. Wendt, and H. E. Hunziker, "ND₄ Schüler band absorption observed by laser FM spectroscopy in a photochemical reaction," *J. Chem. Phys.* **80**, 961 (1984).
 38. G. Herzberg, "Rydberg spectra of triatomic hydrogen and of the ammonium radical," *Faraday Disc. Chem. Soc.* **71**, 165 (1981).
 39. F. Alberti, K. P. Huber, and J. K. G. Watson, "Absorption spectrum and analysis of the ND₄ Schüler band," *J. Mol. Spectrosc.* **107**, 133 (1984).
 40. J. M. Jasinski, E. A. Whittaker, G. C. Bjorklund, R. W. Dreyfus, R. D. Estes, and R. E. Walkup, "Detection of SiH₂ in silane and disilane glow discharges by frequency modulation absorption spectroscopy," *Appl. Phys. Lett.* **44**, 1155 (1984).
 41. M. Romagnoli, M. D. Levenson, and G. C. Bjorklund, "Frequency-modulation-polarization spectroscopy," *Opt. Lett.* **8**, 635 (1983).
 42. M. Romagnoli, M. D. Levenson, and G. C. Bjorklund, "Frequency-modulation-polarization-spectroscopy detection of persistent spectral holes," *J. Opt. Soc. Am. B* **1**, 571 (1984).
 43. M. Gehrtz, W. E. Moerner, and G. C. Bjorklund, "Shot-noise limited detection of very weak absorptions with laser FM spectroscopy," *Opt. Lett.* (to be published).
 44. This is the most important difference between this method and the double-beam WMS scheme proposed in Ref. 14, where the corresponding phase shift is 90°.
 45. Cf. the much more complicated demodulation scheme used in the double-beam, one-detector WMS method proposed by M. Welkowsky and R. Braunstein, "A double-beam, single-detector wavelength modulation spectrometer," *Rev. Sci. Instrum.* **43**, 399 (1972).
 46. K.-H. Hellwege, ed., *Landolt-Börnstein Zahlenwerte und Funktionen* (Springer-Verlag, Berlin, 1960), Vol. II-2a, p. 10.
 47. As the width of the absorption line depicted in Fig. 12 is somewhat larger than the FM sideband spacing, the maximum differential absorption experienced by the sidebands is slightly smaller than the peak absorptivity of the line. Although the corresponding reduction factor could be calculated explicitly from the FM line-shape theory,²⁸ we chose a calibration procedure^{29,35} that for a given linewidth relates the FM-signal voltage directly to the peak absorptivity. The values that we quote here and in Fig. 12 thus correspond to absorptivity differences taken at the absorption line peak and at a position off the absorption line.
 48. The widths of the absorption lines shown in Fig. 13 are slightly smaller than the FM sideband spacing. Thus in this case the maximum differential absorptivity experienced by the sidebands is directly given by the peak absorptivities of the iodine absorption lines, and the $\Delta\delta$ values that we quote here and in Fig. 13 are exactly equal to the differential absorptivities seen by the sidebands.
 49. The RAM-induced noise spectrum observed previously³⁵ (Fig. 5) shows much stronger low-frequency components, probably for two reasons: (1) A different EOM was used that caused much stronger RAM and (2) a relatively high FM index ($M \sim 1$) was employed that also increased the RAM.
 50. J. F. Ward, C. C. Wang, and C. E. Wieman, "A proposal for improved OH detection using frequency modulation spectroscopy," presented at the March 1985 meeting of the American Physical Society, Baltimore, Maryland.
 51. L. T. Molinari and W. B. Grant, "FTIR-spectrometer-determined absorption coefficients of seven hydrazine fuel gases: implications for laser remote sensing," *Appl. Opt.* **23**, 3893 (1984).
 52. D. E. Cooper and T. F. Gallagher, "Frequency modulation spectroscopy with a CO₂ laser: results and implications for ultrasensitive point monitoring of the atmosphere," *Appl. Opt.* **24**, 710 (1985).
 53. P. A. Leighton, *Photochemistry of Air Pollution* (Academic, New York, 1961).
 54. K. A. Frederiksson and H. M. Hertz, "Evaluation of the DIAL technique for studies on NO₂ using a mobile lidar system," *Appl. Opt.* **23**, 1403 (1984).
 55. H. Levy II, "Photochemistry of the troposphere," *Adv. Photochem.* **9**, 369 (1974).
 56. D. K. Hsu, D. L. Monts, and R. N. Zare, *Spectral Atlas of Nitrogen Dioxide 5530 Å to 6480 Å* (Academic, New York, 1978).
 57. J. C. D. Brand, W. H. Chan, and J. L. Hardwick, "Rotational analysis of the 8000–9000 Å bands of nitrogen dioxide," *J. Mol. Spectrosc.* **56**, 309 (1975).

(see overleaf)

Manfred Gehrtz



Manfred Gehrtz was born in Buchloe, West Germany, in 1951. He received the *Diplom-Physiker* degree from the University of Munich in 1980. His thesis work was conducted at the Institute of Physical Chemistry of the University of Munich and concerned optical detection of magnetic resonance investigations of solid-state photophysical and photochemical processes at liquid-helium temperatures. He received his *Dr. rer. nat.* degree in 1983. Between 1983 and 1985, Dr. Gehrtz was an IBM World

Trade Visiting Scientist at the IBM Research Laboratory in San Jose, California. There he worked on materials for frequency-domain optical memories based on spectral hole burning, and on laser FM spectroscopy. Dr. Gehrtz is a member of the Deutsche Physikalische Gesellschaft and the American Physical Society.

Edward A. Whittaker



Edward A. Whittaker was born in LaPorte, Indiana, in 1953. He received the B.S. degree in physics from Worcester Polytechnic Institute, Worcester, Massachusetts, in 1976. His Ph.D. research in photon echo modulation spectroscopy was carried out at Columbia University, where he received his degree in 1982. He spent two years as a visiting scientist at IBM San Jose Research Laboratory doing research in FM spectroscopy and is now an assistant professor at Stevens Institute of Technology, where

he plans to continue research in laser spectroscopy and applied optics.

Gary C. Bjorklund



Gary C. Bjorklund is manager of Laser Materials Interactions at the IBM San Jose Research Laboratory. He did his undergraduate work at the Massachusetts Institute of Technology, where he received the B.S. degree in physics in 1968, and his graduate work at Stanford University, where he received the M.S. and Ph.D. degrees in applied physics in 1969 and 1974. His thesis research, performed under Professor S. E. Harris, concerned nonlinear optics in gases and vacuum-ultraviolet holography. From

1974 to 1979, he was a member of the Technical Staff at Bell Laboratories, where he performed research on nonlinear optics and laser spectroscopy. In 1979 Dr. Bjorklund joined the IBM San Jose Research Laboratory, where his personal research interests have been in applications of nonlinear optics and laser spectroscopy for holography, sensitive detection, and optical information storage. In 1980 he became manager of quantum electronics, in 1983 became manager of optical storage science and technology, and in 1985 he assumed his present position. Dr. Bjorklund is a senior member of the Institute of Electrical and Electronics Engineers (IEEE), a member of the Optical Society of America, and a member of the American Physical Society (APS). He has served as an executive committee member of the APS Division of Electron and Atomic Physics and on the administrative committee of the IEEE Lasers and Electro-Optics Society (LEOS). During 1985 he will be vice president of LEOS. He served as cochairman of the program committee for the 1984 Conference on Lasers and Electro-Optics (CLEO) and will be general cochairman of the 1986 CLEO.